

# Generation of attosecond unidirectional half-cycle pulses: Inclusion of propagation effects

E. Persson,<sup>1</sup> K. Schiessl,<sup>1</sup> A. Scrinzi,<sup>2</sup> and J. Burgdörfer<sup>1</sup>

<sup>1</sup>*Institute for Theoretical Physics, Vienna University of Technology, A-1040 Vienna, Austria*

<sup>2</sup>*Institute for Photonics, Vienna University of Technology, A-1040 Vienna, Austria*

(Received 3 February 2006; published 31 July 2006)

Unidirectional half-cycle pulses (HCP) are ideally suitable for shaping, driving, and probing atomic wave packets in momentum space. The shortest HCP presently available have a width of about 500 fs restricting the manipulation of electronic wave packets to those in high-lying Rydberg states. The nonlinear harmonic response of atoms to strong two-color infrared laser pulses with frequencies  $\omega$  and  $2\omega$  opens up the opportunity to form trains of ultrafast HCP's on an attosecond time scale. In the present contribution, we investigate the influence of macroscopic propagation effects onto the production of HCP and show that trains of unidirectional attosecond HCP's could be produced under experimentally realistic conditions.

DOI: [10.1103/PhysRevA.74.013818](https://doi.org/10.1103/PhysRevA.74.013818)

PACS number(s): 42.65.Re, 32.80.Wr

## I. INTRODUCTION

The shortest electromagnetic pulses presently available are obtained from high-order harmonics generation (HHG) through the nonlinear interaction of a short, high-intensity laser field with a gas jet. Filtering out a few of the highest harmonics leads to pulses with widths as short as some hundreds of attoseconds [1–3]. In view of the very high frequency of the XUV carrier, this electromagnetic pulse still subtends several periods of the carrier oscillation within the envelope. Such a field, referred to as an attosecond burst, is capable of delivering a pulse of photon energy ( $\leq 1000$  eV) on a sub-fs time scale. By contrast, a half-cycle pulse (HCP) contains ideally no additional oscillatory structure inside its envelope. If the width  $\tau_p$  of such a pulse is short compared to the typical time scale  $T_n$  of the driven system, the HCP is impulsive, i.e., it delivers a linear momentum to an electron. Figure 1 illustrates similarities and differences between an idealized train of unidirectional HCP's (UHCP's) and a train of attosecond bursts.

The motivation to generate HCP's on the attosecond scale is derived from the study of coherent state manipulation in Rydberg atoms employing HCP's. Two HCP's in a pump-probe setting can be used to impulsively tailor and detect wave packets [4,5], and to retrieve quantum information [6]. By chirping the period and field strength of a train of UHCP's, it is possible to steer an electronic wave packet towards a preferred region in phase space [7]. In the Rydberg atom exposed to a periodic train UHCP, dynamical localization is observed [8,9]: the wave function of the driven system remains close to the initial state for a long time even though the driving field is strong, allowing us to keep the wave function in the preferred region of phase space for many cycles of the driving field.

Presently, two methods for producing single HCP or trains of HCP's are being used. By a conventional pulse generator, pulse widths down to  $\tau_p \approx 500$  ps can be achieved [10]. Applying a large voltage across a semiconductor wafer and short-circuiting it by electron-hole excitations in a strong fs laser, HCP's with widths  $\tau_p \approx 500$  fs can be produced [11]. Such HCP's reach the impulsive limit  $\tau_p \ll T_n$  only for Rydberg states with  $n \gg 1$ , where the typical time scale

$T_n = h/\Delta E = 0.16 \text{ fs} \times n^3$  with  $\Delta E$  the level spacing of the Rydberg states ( $n \approx 30$  for sub-ps pulses and  $n \approx 300$  for sub-ns pulses).

Reaching the impulsive limit for the electronic ground state of atoms, molecules, or solids requires attosecond (as)

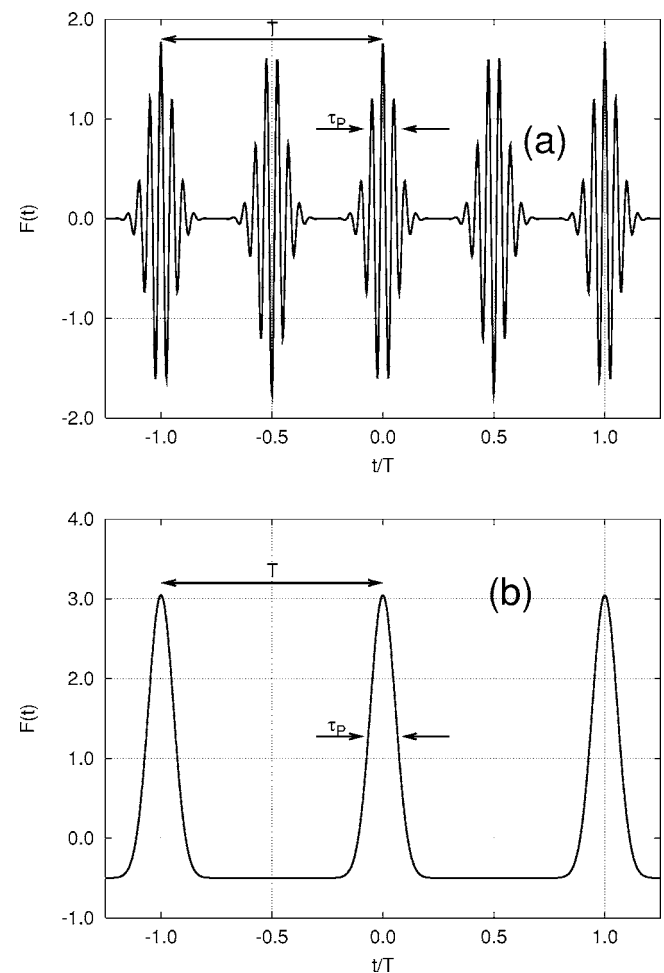


FIG. 1. A train of attosecond bursts (a) and a train of UHCP's (b) in units of the period  $T = 2\pi/\omega$  of the fundamental color. In both cases, the width of the individual pulses is  $\tau_p = 0.18 T$  and the time-averaged field  $f_0 = 0$ .

pulses. In the present communication, we analyze protocols to generate unipolar as HCP's based on HHG resulting from two-color driving. In a previous preliminary study we have suggested that the nonlinear single-atom response to driving at the fundamental frequency  $\omega_1$  and the second harmonic  $2\omega_1$  results in UHCP's [12]. However, the generation and survival of such pulses under realistic macroscopic propagation conditions in a gaseous medium has not yet been addressed. We present in the following simulations for the protocol to generate UHCP's and focus on the role of macroscopic propagation effects. The simulations are based on a self-consistent coupling of the atomic Schrödinger equation and Maxwell's equations for the electromagnetic pulse in the medium. We consider hydrogen and argon gas targets and calculate the intensities and pulse shapes to be expected. The layout of the paper is as follows: In Sec. II we introduce the method used for the simulations. The numerical results of our studies are presented in Sec. III followed by conclusions and outlook in Sec. IV.

## II. METHOD

We consider in the following the propagation of few-cycle laser pulses through a gaseous medium. The propagation is taken to be along the  $x$  direction while the laser field is linearly polarized along the  $z$  axis. We study the nonlinear atomic response to the electromagnetic field, which will be self-consistently coupled to the optical field. Maxwell's equations with sources will be coupled to the fully quantum-mechanical response of the atomic medium. Similar self-consistent couplings have been used, in, e.g., [13]. The high-harmonic radiation, both generated and propagated, will be optimized towards the goal to shape unidirectional half-cycle pulses (UHCP's) on the attosecond time scale.

The wave equation for linearly polarized electric field  $F_z = F$  in the presence of a polarizable medium with nonlinear polarization  $P(x, t)$  is given by

$$\left( \frac{\partial^2}{\partial x^2} - \frac{1}{c^2} \frac{\partial^2}{\partial t^2} \right) F(x, t) = \frac{4\pi}{c^2} \frac{\partial^2}{\partial t^2} P(x, t). \quad (1)$$

We neglect the dependencies of  $F$  and  $P$  on the coordinates transverse to the propagating direction since we are studying the far field in the propagation direction. This is justified by assuming that the wavelength  $\lambda_1$  of the fundamental harmonic is small compared to the diameter of the laser beam which, in turn, is smaller than that of the gas jet. For the present protocol, to be discussed below, intensities for the fundamental driving field of no more than  $10^{14}$  W/cm<sup>2</sup> are sufficient. Therefore the requirements on beam focusing are modest. A minimum beam waist of  $W_0$  about a few 100  $\mu$ m is sufficient for pulse energies in the order of several 10 nJ. In turn, the phase changes due to a curvature of the wave front can be neglected. The corresponding coherence length from the Guoy-phase,  $L_{\text{Guoy}} = \pi^2 W_0^2 / n \lambda_1$  [15] (with  $n$  the order of the harmonics,  $n < 10$ ), is much longer than the propagation lengths studied in this paper. While diffraction may lead to deviation from the one-dimensional (1D) approximation at large distances from the generation region, the 1D

approximation is justified for the present loose-focusing geometry and experimentally relevant distances.

We first take the Fourier transform in time of Eq. (1) and insert the ansatz to separate rapidly oscillating phases in position coordinate,

$$F(x, \omega) = e^{-i\omega x/c} F^{\text{slow}}(x, \omega),$$

$$P(x, \omega) = e^{-i\omega x/c} P^{\text{slow}}(x, \omega). \quad (2)$$

Neglecting  $\partial^2 F^{\text{slow}}(x, \omega) / \partial x^2$  leads to the first-order propagation equation

$$\frac{\partial F^{\text{slow}}(x, \omega)}{\partial x} = -i \frac{2\pi\omega}{c} P^{\text{slow}}(x, \omega), \quad (3)$$

which is an adequate approximation to Eq. (1) as long as backwards-propagating solutions of the latter can be neglected [14]. This is justified in the case of propagation through low-pressure gas jets used for harmonic generation, as studied in this contribution. Equation (3) will be solved numerically by a slice-by-slice propagation with a slice width  $\Delta x$ . We define a useful generalization of the position-dependent susceptibility as

$$\chi(x, \omega) = \frac{P(x, \omega)}{F(x, \omega)}. \quad (4)$$

For linear processes  $\chi$  reduces to the linear susceptibility  $\chi(x, \omega) \rightarrow \chi_L(\omega)$ , independent of  $F(\omega)$  and the position  $x$ . In our method the generally non-linear  $\chi(x, \omega)$  will be determined by the full quantum-mechanical response  $P^{\text{slow}}(x, \omega)$  of the atomic medium.

It is instructive to consider limiting cases for which analytic solutions of Eq. (3) become feasible. The latter can also be used to speed up the numerical propagation. To underline the different contributions to the nonlinear response,  $P^{\text{slow}}(x, \omega)$  is approximated in a small interval  $[x_0, x_0 + \Delta x]$  as

$$P^{\text{slow}}(x, \omega) = P_d^{\text{slow}}(x_0, \omega) + \chi_A(x_0, \omega) F^{\text{slow}}(x, \omega). \quad (5)$$

The ansatz can be motivated as follows:  $P_d^{\text{slow}}$  for the higher harmonics originates from the strong driving laser and is thus constant as long as the driving components do not change. Due to the low intensities of the higher harmonics, the approximate  $\chi_A(x, \omega) \approx \chi_L(\omega)$ , where  $\chi_L(\omega)$  is the linear susceptibility being independent of the field. On the other hand, for the strong driving frequencies ( $\omega_1$  or  $\omega_2$ )  $P_d^{\text{slow}}$  is practically zero and  $\chi_A(x, \omega) \approx \chi(x, \omega)$  with  $\chi(x, \omega)$  the non-linear susceptibility, which is dependent on the intensity, generally. Thus,  $P_d^{\text{slow}}(x, \omega)$  as well as  $\chi_A(x, \omega)$  can be considered as practically constant for all frequencies studied as long as  $\Delta x$  is small compared to the absorption length of the driving colors. With the ansatz (5), Eq. (3) can be solved analytically as

$$F^{\text{slow}}(x_0 + \Delta x, \omega) = \exp\left(-i \frac{2\pi\chi_A(x_0, \omega)\omega\Delta x}{c}\right) \left( F^{\text{slow}}(x_0, \omega) + \frac{P_d^{\text{slow}}(x_0, \omega)}{\chi_A(x_0, \omega)} \right) - \frac{P_d^{\text{slow}}(x_0, \omega)}{\chi_A(x_0, \omega)}. \quad (6)$$

Two limiting cases of Eq. (6) are of interest: For  $x \rightarrow 0$  and  $F^{\text{slow}}(x_0, \omega)$  small,

$$F^{\text{slow}}(x_0 + \Delta x, \omega) = F^{\text{slow}}(x_0, \omega) - i \frac{2\pi\omega}{c} P^{\text{slow}}(x_0, \omega) \Delta x + O\left(\frac{\omega^2 P_d^{\text{slow}} \chi_A \Delta x^2}{c^2}\right), \quad (7)$$

while for  $F^{\text{slow}}(x_0, \omega)$  large, Eq. (6) leads to

$$F^{\text{slow}}(x_0 + \Delta x, \omega) = \exp\left(-i \frac{2\pi\chi(x_0, \omega)\omega\Delta x}{c}\right) F^{\text{slow}}(x_0, \omega) + O\left(\frac{\omega^2 (P_d^{\text{slow}})^2 \Delta x^2}{c^2 F^{\text{slow}}(x_0)}\right), \quad (8)$$

where  $\chi(x, \omega)$  is the full nonlinear response from Eq. (4).

The numerical propagation in steps  $x_j$  with the slice width  $\Delta x_j = x_j - x_{j-1}$  is accelerated by iteratively applying either Eq. (7) or Eq. (8). Since both equations are accurate in  $\Delta x_j$  to the order  $O(\Delta x_j^2)$ , they can be smoothly matched provided  $\Delta x_j$  is small enough. Due to the contribution of  $1/F^{\text{slow}}$  to the error term of Eq. (8), we can use larger  $\Delta x_j$  by applying Eq. (7) for small  $x$  (i.e., small  $F$  for the higher harmonics), and Eq. (8) for large  $x$  (large  $F$ ).

The nonlinear polarization response entering Eqs. (7) and (8) is determined from the concurrently solved time-dependent Schrödinger equation (TDSE) for a single-active electron (SAE). The TDSE

$$i \frac{\partial}{\partial t} \psi(\vec{r}, t) = [H_0 + z F^{\text{slow}}(t)] \psi(\vec{r}, t) \quad (9)$$

contains the atomic Hamiltonian,

$$H_0 = \frac{p^2}{2} + V_{\text{eff}}(r), \quad (10)$$

with  $V_{\text{eff}}(r)$  the atomic potential, in the following to be taken either hydrogenic [ $V_{\text{eff}}(r) = -1/r$ ] or a parametrized model potential for argon (Sec. III C). Equation (9) determines the microscopic response in the dipole approximation employing the length gauge. We integrate the TDSE on a finite grid by means of the pseudospectral method [16]. In this method, the integration is performed applying a split-operator method,

$$\Psi(t + \Delta t) = \exp(-i\Delta t H_0/2) \exp(i\Delta p_j \hat{z}) \exp(-i\Delta t H_0/2) \Psi(t) + O(\Delta t^3), \quad (11)$$

with  $\Delta p_j = -\int_t^{t+\Delta t} F^{\text{slow}}(t) dt$ . The  $r$  coordinate is discretized on  $[0, r_{\text{max}}]$  at points  $r_i$  optimized for the usage of effective quadrature methods for the evaluation of the matrix elements in Eq. (11). Accurate solutions of the TDSE are obtained using a small number of points in  $r$  (typically about 200 for intensity  $I \sim 10^{14}$  W/cm<sup>2</sup> at a wavelength  $\lambda \sim 1000$  nm). A

smooth cutoff function  $f(r)$  is multiplied to the wave function in each time step to avoid spurious reflections at the border at  $r_{\text{max}}$ . Due to the absorption of probability at large  $r$ , the norm  $N$  of the wave function,

$$N(t) = \langle \Psi(t) | \Psi(t) \rangle, \quad (12)$$

is decaying with time. Accordingly, the fraction of lost electrons due to ionization,  $1 - N(t)$ , gives rise to a density of free electrons,  $n_{\text{free}} = n_a [1 - N(t)]$ , where  $n_a$  is the atomic density. Throughout this paper we use the number density  $n_a = 3.6 \times 10^{-7}$ , which corresponds to a pressure of 0.1 atmospheres at temperature 300 K.

From the solution of the TDSE, the polarization of the medium can be calculated. The polarization consists of the time-dependent atomic polarization  $P_a^{\text{slow}}(t)$  and the polarization of the plasma of free electrons generated,

$$P^{\text{slow}}(t) = P_a^{\text{slow}}(t) + P_{\text{free}}^{\text{slow}}(t). \quad (13)$$

$P_a^{\text{slow}}$  is determined by the norm decaying state  $\psi(t)$ ,

$$P_a^{\text{slow}}(t) = n_a \langle \psi(t) | \hat{z} | \psi(t) \rangle. \quad (14)$$

For the polarization of the electron plasma we employ a generalization of the Drude model taking into account the frequency components to  $P_{\text{free}}^{\text{slow}}$  due to the time dependence  $n_{\text{free}}$ ,

$$P_{\text{free}}^{\text{slow}}(t) = -n_{\text{free}}(t) \mathcal{F}^{-1} \left[ \frac{F^{\text{slow}}(\omega)}{\omega^2} \right]. \quad (15)$$

The Fourier transform of  $P^{\text{slow}}(t)$ , Eq. (13), together with Eqs. (7) and (8) results in the self-consistent coupling of the wave equation and the Schrödinger equation. We typically need  $j_{\text{max}} = 200$  steps in the propagation direction  $x$  for a propagation length of 16 mm.

### III. RESULTS FOR HCP SHAPING

#### A. Control parameters for the driving pulse

We first consider the interaction of a two-color laser field with a gas of atomic hydrogen ( $V = -1/r$ ). Two-color driving is required to break the inversion symmetry and to obtain both odd and even harmonics. We parametrize the vector potential of the two-color drive as

$$A(t) = a(t) \left( \frac{(1 - A_R)}{\omega} \sin(\omega t) + \frac{A_R}{2\omega} \sin(2\omega t + A_\phi) \right) \quad (16)$$

with  $\omega = \omega_1$  the fundamental driving frequency,  $a(t)$  an envelope function, and  $A_R$  and  $A_\phi$  the relative amplitude and phase of the second harmonic. The corresponding electric field is given by

$$F(t) = -\frac{1}{c} \frac{dA(t)}{dt}. \quad (17)$$

We search now for optimal driving conditions both in terms of the laser parameters Eq. (16) as well as propagation length  $x$  for generating the output field that resembles that of a train of UHCP's.

An “ideal” UHCP train would have a Fourier decomposition

$$F_{UHCP} = f(t) \left( f_0 + \sum_{n=1} f_n \cos(n\omega t + \phi_n) \right) \quad (18)$$

with  $f(t)$  an envelope function and  $f_n$  the amplitude of the harmonic components. The phases of the harmonic components (with both odd and even present) should be aligned as

$$\phi_n = k\pi + n\Delta\phi \quad (19)$$

with  $k$  an integer and  $\Delta\phi$  related to a time delay as  $\Delta t = -\Delta\phi/\omega$ . With  $k$  even, the HCP are pointing in the positive  $z$  direction (i.e., the direction of the maximum of the driving field) and with  $k$  odd, they point in the negative  $z$  direction. Ideally,  $f_n$  is almost constant for the first few  $n$  before decreasing for the high harmonic order  $n \gg 1$ . If the amplitudes of the harmonics decrease as

$$f_n = \exp[-(n/n_0)^2], \quad (20)$$

corresponding to a Gaussian shape of the individual HCP's, a minimum of field fluctuations between the HCP's results. The damping of the high harmonics controlled by  $n_0$  is related to the temporal FWHM of each individual Gaussian HCP by  $\tau_F = 4\sqrt{\ln 2}/(\omega n_0)$ . A zero-frequency component of  $f_0 = \frac{1}{2}$  that appears for an ideal UHCP and is realized by electric pulse generators [10] cannot be present for a freely propagating wave. We will, therefore, search for an output pulse resembling Eq. (18), however with  $f_0 = 0$ . For Rydberg states it has been shown that the absence of an average field changes the dynamics close to and above the ionization threshold while being immaterial for the dynamics close to the initial state [17]. An example of an ideal train of HCP's with Gaussian shape of the individual HCP's is show in Fig. 1.

### B. Results for hydrogen

We present in the following a few examples of UHCP output fields. In the first case (Fig. 2) we study propagation through a hydrogen gas of a driving field with intensity  $I_D = 10^{14}$  W/cm<sup>2</sup> and fundamental wavelength  $\lambda_1 = 1064$  nm. Here and in the following we express the intensity (in atomic units) of the driving field in terms of the maximum of the field,  $I_D = \max[F(t)]^2/2$  and the intensity  $I_n$  of the different harmonics with respect to the maximum of the individual harmonics,  $I_n = \max[F_n(t)]^2/2$  with  $F_n(t)$  the time-dependent field corresponding to harmonic  $n$ . The result presented in Fig. 2 was found by a scan over  $A_R$  and  $A_\phi$  [see Eq. (16)].

Figure 2(a) displays the few-cycle flat-top driving field. Around the frequency corresponding to resonant coupling to the first excited state, the power spectrum [Fig. 2(b)] in the single atom response approximation [defined via Eq. (8)] is strongly enhanced. Including propagation through the gas, strong absorption at the resonance takes place leading to a much lower radiation close to the resonance. The nonlinear response of the medium mimics the UHCP requirements Eq. (18) both in terms of the harmonic intensities as well as the phases quite well [Fig. 2(c)]. The only mismatch is caused by

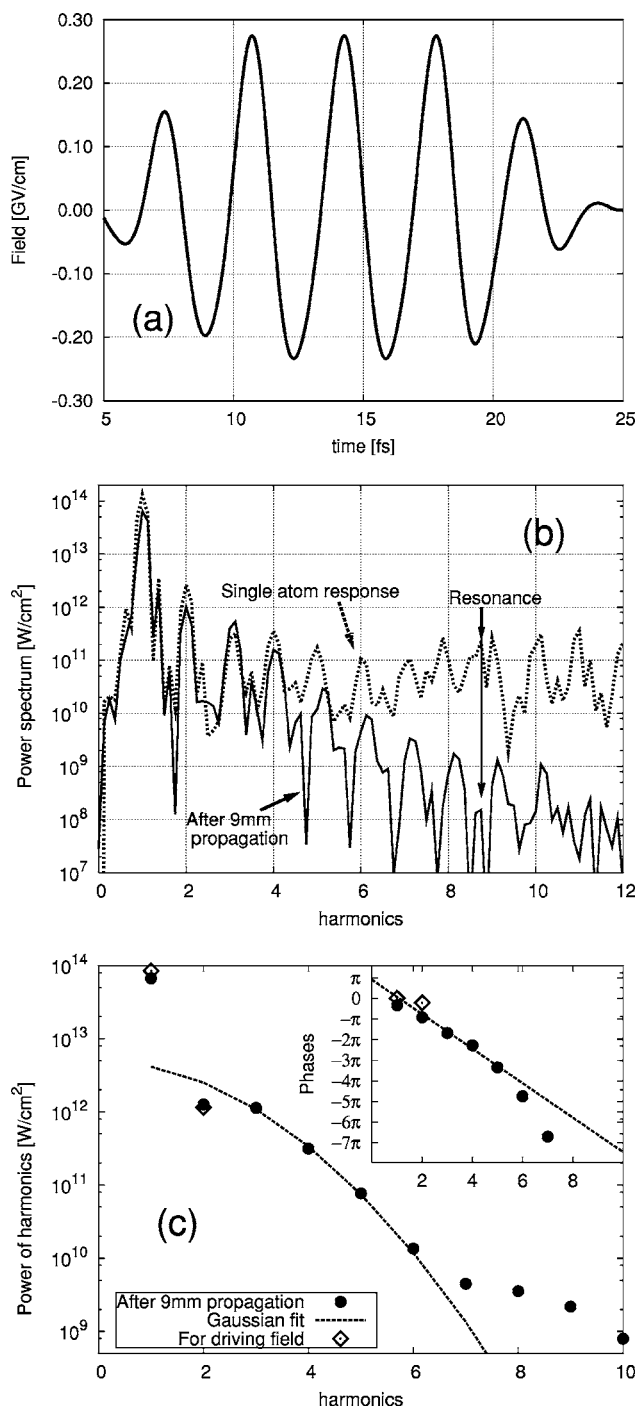


FIG. 2. (a) The few-cycle flat-top driving pulse with  $I_D = 1 \times 10^{14}$  W/cm<sup>2</sup>,  $A_R = 0.1$ ,  $A_\phi = -0.7$ , and  $\lambda_1 = 1064$  nm. (b) Power spectrum after 9 mm propagation through hydrogen (full line) compared to that of the single-atom response Eq. (7), dashed line. (c) Intensities and phases (inset) of the harmonics as found after 9 mm propagation (points). Dashed lines: Dependence for an optimal train of UHCP, [see Eq. (18); the individual HCP's are assumed Gaussian, Eq. (20)]. Diamonds: values for the driving field.

the strong dominance of the original driving field at the fundamental wavelength  $\lambda_1$ . We will assume that the intensities and phases of the two driving colors can be appropriately adjusted after the HHG in the gaseous medium. For compari-

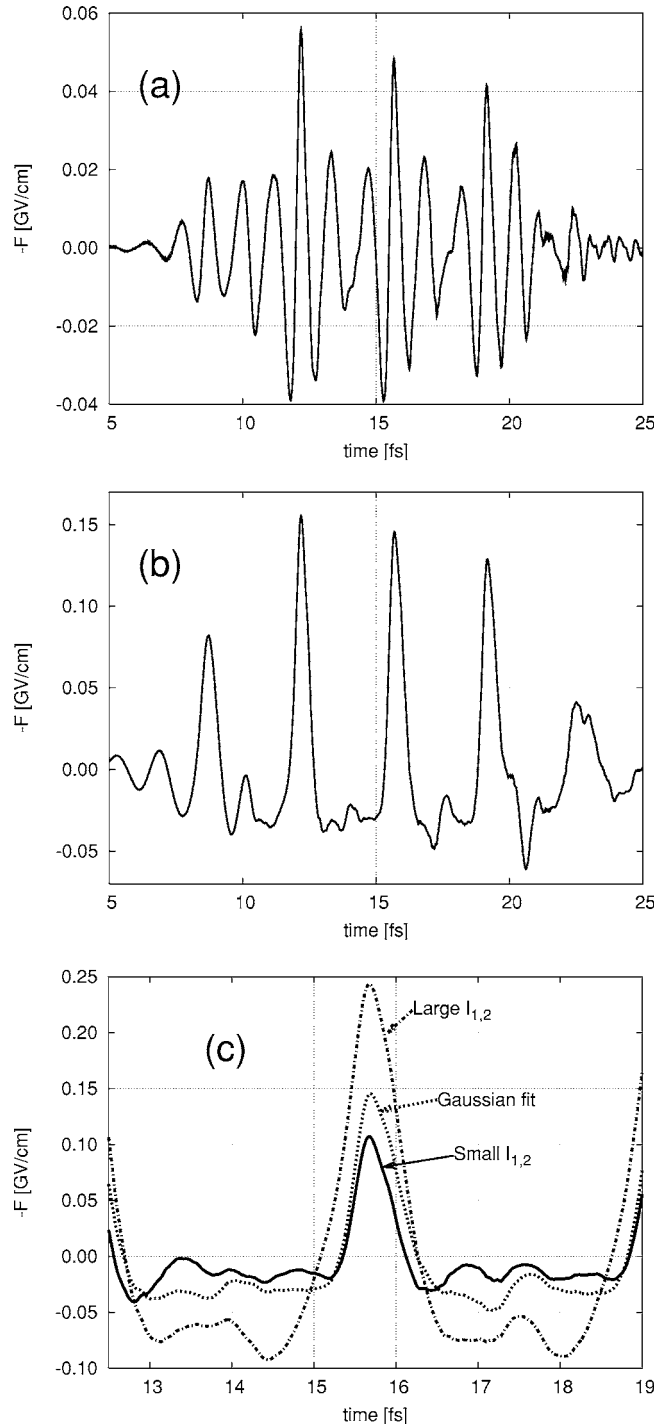


FIG. 3. (a) Generated field after completely removing the two driving components. (b) Pulse after adjustment of the intensities and phases of the two driving colors according to Eqs. (18) and (20). (c) Magnification of the field in (b) compared with two other choices of the intensity adjustments (see text for details). The propagation length  $x=9$  mm and the driving field is the same as in Fig. 2(a).

son, we present in Fig. 3(a) the field resulting when completely removing the two driving colors. The resulting field after adjustment of the two driving colors, displayed in Fig. 3(b), resembles a train of UHCP [Fig. 1(b)] quite well. The train has an intensity of  $I_{HCP}=4.2 \times 10^{12}$  W/cm<sup>2</sup> and width

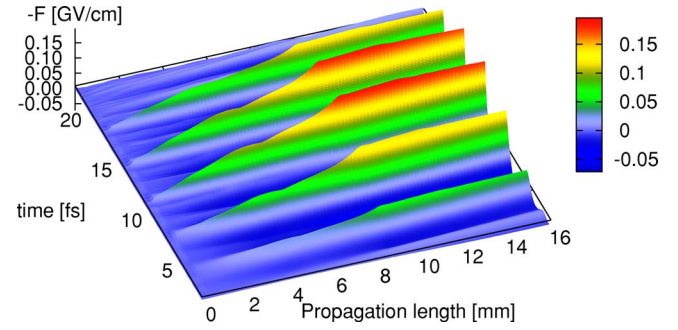


FIG. 4. (Color online) Train of UHCP for different propagation lengths. The driving components are adjusted to a Gaussian and the driving field is the same as in Fig. 2(a).

$\tau_p$  (FWHM) of the individual HCP's as directly determined from  $F_{UHCP}$ ,  $\tau_p=650$  as. The ratio of the width to the optical cycle,  $T=3.5$  fs,  $\tau_p/T=0.18$  characterizes the temporal width of the HCP spikes in the electrical field. The width is effectively controlled by the number of harmonics that can be phase-aligned and follow an appropriate exponential decay of the intensity with  $n$ . The number of phases possible to align is limited by the frequency necessary for resonant coupling to the first excited state  $2p$ , corresponding to harmonics  $n \approx 8$  in Fig. 2(b).

We note that the existence of HCP's in the trains is not critically dependent on the exact choice of intensity adjustments of the two driving colors [Fig. 3(c)]. Without adjusting the intensity of the second color but adjusting the intensity of the first color to that of the second color and the phases for both colors, a train of HCP's (full line) with somewhat lower intensity of the train,  $I_{HCP}=1.3 \times 10^{12}$  W/cm<sup>2</sup>, but also with narrower spikes,  $\tau_p=550$  as, is found. On the contrary, choosing the intensities of the two driving colors a factor 2 stronger than the Gaussian fit (dashed-dotted line) the intensity of the UHCP train doubles, but also the width of the HCP's increases to  $\tau_p=790$  as.

The degree of unipolarity of the field can be characterized by the directionality of the ionization. Even though the integral of the field presented in Fig. 3(b) is zero, the total ionization is strongly asymmetric: By solving the time-dependent Schrödinger equation, we find about 5 times more ionization during the spikes as compared to the smooth field in the opposite direction. The evolution of the UHCP train as a function of propagation distance  $x$ , displayed in Fig. 4, shows that in the present case an optimum in terms of amplitude is reached near  $x=9$  mm.

As an example for the dependence of the HCP output on various driving parameters, we present the dependence on the driving intensity  $I_D$  under otherwise identical conditions in Fig. 5. The intensities of the higher harmonics [Fig. 5(a)] decreases rapidly with the intensity  $I_D$  due to the strong non-linearity of the process of harmonic generation. For the lowest intensity studied, the intensity of the first harmonic with frequency  $\omega_1$  after propagation is a factor of 190 too large relative to the desired intensity for a UHCP [Eq. (18)], when requiring a Gaussian dependence of  $f_n$ . For  $I_D=1 \times 10^{14}$ ,  $f_1$  is 23 too large, i.e., the intensity fraction that has to be filtered out is a factor of 8 smaller for the stronger driving field.

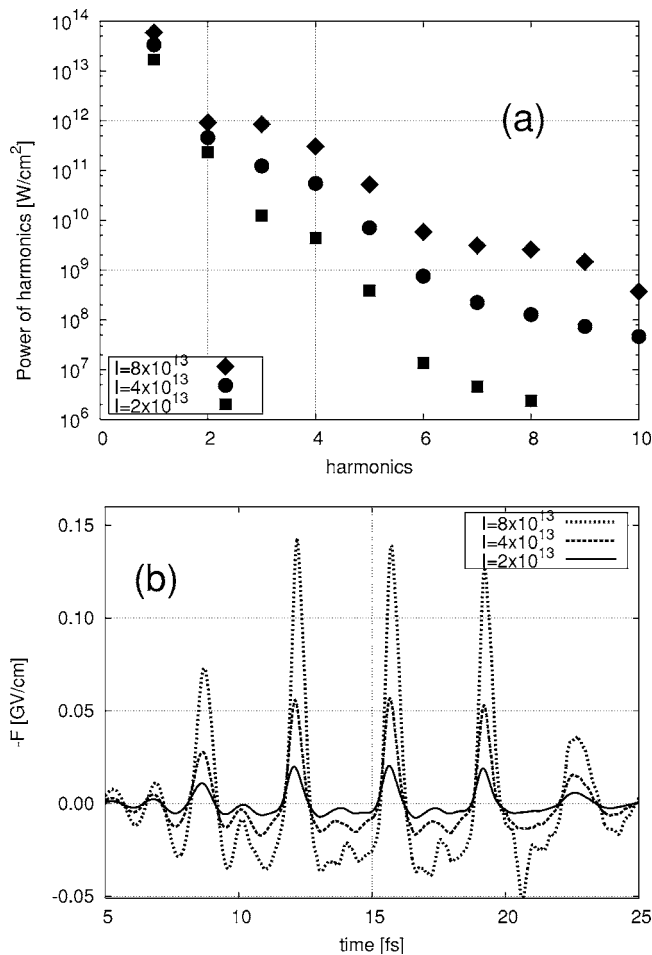


FIG. 5. (a) Intensities of harmonics and (b) the resulting field after 9 mm propagation for different intensities. The driving components are adjusted to a Gaussian and the driving field is the same as in Fig. 2(a).

Together with the fact that there is considerable flexibility concerning the exact intensity adjustment of the driving intensities [Fig. 3(c)] it thus seems possible to find experimental means of adjusting the two driving colors provided the intensity is high enough.

The present scheme for producing UHCP can be extended to longer pulses encompassing a larger number of spikes. The extension is, however, limited by the increased ionization for longer pulses. When using a 30 cycles long field with  $I_D = 1 \times 10^{14} \text{ W}/\text{cm}^2$  ionization on a 15% level results. Due to the strong distortion caused by free electrons, we were not able to find a well-defined train of UHCP in this case. At lower intensities ( $I_D = 5 \times 10^{13} \text{ W}/\text{cm}^2$ ) the ionization for  $x \rightarrow 0$  is reduced 5.5%, and further reduced at  $x = 9 \text{ mm}$  to 2.5%. In this case a train of UHCP extending over 30 pronounced spikes as shown in Fig. 6 results.

It is also of interest to explore the wavelength dependence of the UHCP generation. We, therefore, consider the case  $\lambda_1 = 2148 \text{ nm}$ . The major benefit of the reduction in driving frequency is that more harmonics fit energetically in between the ground state and the first excited state, thus allowing for an increased number of phase-aligned harmonics [Fig. 7(a)]. The downside is a strong reduction in intensity of high har-

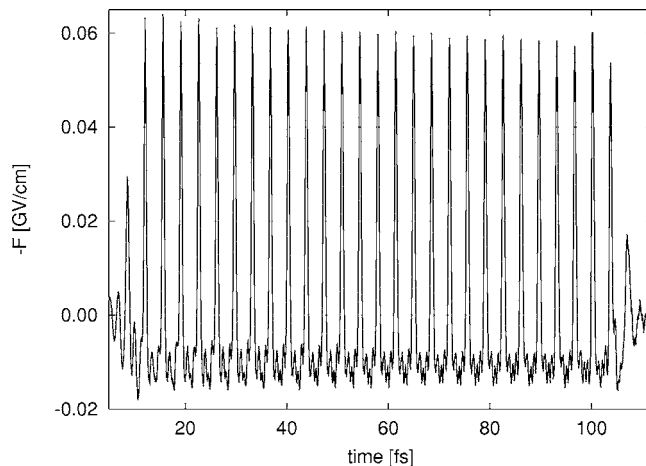


FIG. 6. A 30-cycle train of UHCP generated by a driving pulse with intensity  $I_D = 5 \times 10^{13} \text{ W}/\text{cm}^2$ ; other parameters are as in Fig. 2(a).

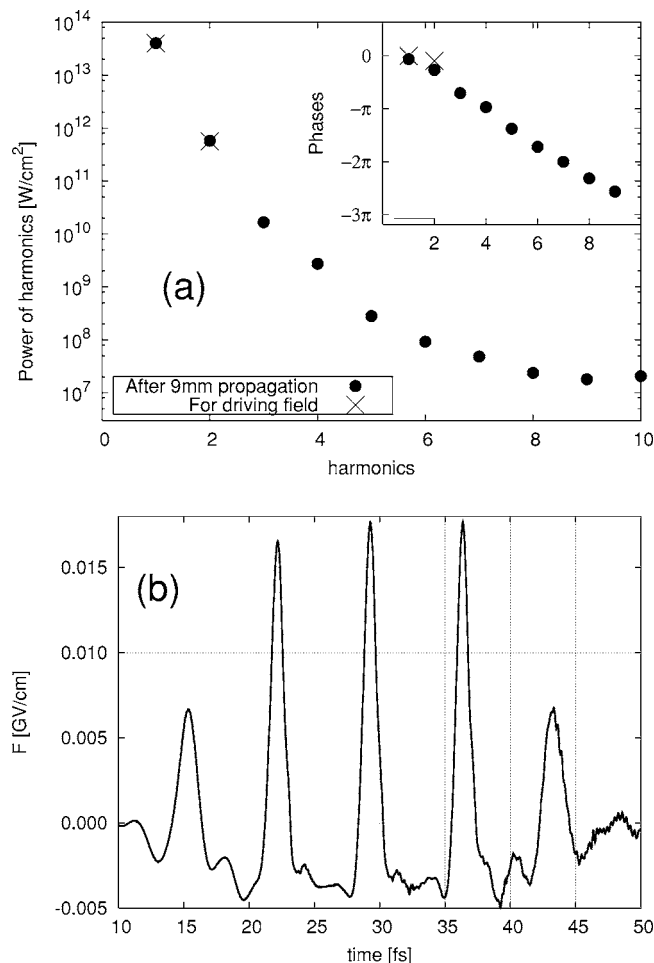


FIG. 7. (a) Harmonic intensity and phase alignment for two-color driving of a hydrogen gas with the fundamental wavelength  $\lambda_1 = 2148 \text{ nm}$ , intensity  $I_D = 5 \times 10^{13} \text{ W}/\text{cm}^2$ , and  $A_\phi = -0.3$ , other parameters are as in Fig. 2. (b) Resulting output field.

monics since a larger number of photons is needed to transfer the electron to the continuum. The train [Fig. 7(b)] has an intensity of  $I_{HCP} \approx 5.7 \times 10^{10} \text{ W/cm}^2$ . The absolute width  $\tau_p \approx 1.1 \text{ fs}$  of each HCP is larger than for the case of driving at  $\lambda_1 = 1064 \text{ nm}$ . This is due to the scaling of  $\tau_p \propto \omega_1^{-1}$  for the same number of aligned harmonics. However, expressed in terms of the period  $T$ ,  $\tau_p/T \approx 0.16$ , the spikes become narrower by a factor 1.2. Further optimization exploring the possibility of obtaining a larger number of aligned harmonics for the case with longer fundamental wavelength appears possible.

### C. Results for argon

So far we have analyzed propagation through a gas jet consisting of hydrogen atoms which allows for the *ab initio* calculation of the atomic response. However, for future experimental realizations propagation in rare gas media is of interest. We therefore study the UHCP generation in argon. We calculate the atomic response within the SAE approximation employing the core potential [18],

$$V(r) = -[1 + 5.4e^{-r} + (17 - 5.4)e^{-3.682r}]/r, \quad (21)$$

which reproduces the relevant bound-state energies ( $3p$ ,  $4s$ ,  $4p$ , and  $4d$ ) within an accuracy of 1%. Since the ground state of argon is the  $3p$  state, we need to block the transition to lower-lying states ( $3s$ ,  $2s$ ,  $2p$ , and  $1s$ ). We achieve this by replacing  $H_0$  in the subspace spanned by the low-lying states by an artificial Hamiltonian submatrix  $\tilde{H}_0$  which leads to a population less than  $10^{-8}$  of the blocked states. The resulting dynamic polarizability  $\alpha(\omega = \omega_1) = 8.7$  is quite close to the experimental value  $\alpha = 10.6$ .

The resulting UHCP train for the same parameters of the driving field as for atomic hydrogen (see Fig. 2) is displayed in Fig. 8. The temporal width of each spike,  $\tau_p = 520 \text{ as}$  ( $\tau_p/T \approx 0.15$ ) is narrower than for hydrogen. This results from the larger number of aligned phases. Their number is limited by the number of harmonics energetically fitting in between the ground state and the first excited state, which is approximately 10 for argon, but only 8 for hydrogen. The output intensity  $I_{HCP} = 2 \times 10^{13} \text{ W/cm}^2$  is a factor of 3 smaller than for hydrogen, which we attribute to the larger ionization potential for argon,  $I_p = 15.8 \text{ eV}$  for argon (versus  $I_p = 13.6 \text{ eV}$  for hydrogen). Evidently, the basic properties of generation and propagation of UHCP trains for rare gases are very similar to those of atomic hydrogen.

## IV. SUMMARY AND OUTLOOK

We investigated in this paper a protocol for producing UHCP in the attosecond regime. In our simulations, we take both the fully quantum-mechanical single-atom response as well as macroscopic propagation effects into account by cou-

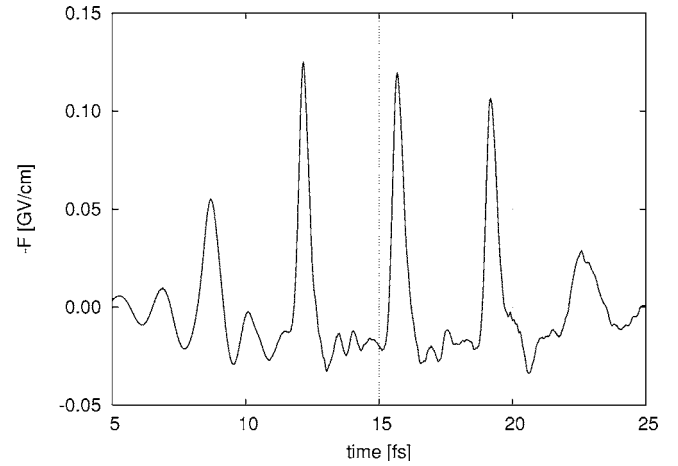


FIG. 8. Train of UHCP after  $x = 5.4 \text{ mm}$  propagation through argon. The parameters of the driving field are as in Fig. 2(a).

pling the solution of the time-dependent Schrödinger equation to the solution (in 1D) of Maxwell's equations. Our proposal consists of a strong infrared laser with fundamental frequency  $\omega$  and a small admixture of the frequency doubled component  $2\omega$  interacting with a gas jet to produce odd and even harmonics. By carefully choosing the length of the gas target and the parameters of the two-color driving field, the harmonics generated up to the frequency corresponding to the excitation from the ground state to the first excited state can be tuned to what is needed for the UHCP. The two driving components have to be tuned after the harmonic production to the appropriate intensities and phases. Using a fundamental wavelength  $\lambda = 1064 \text{ nm}$  and intensities of the driving field up to  $I_D = 1 \times 10^{14} \text{ W/cm}^2$  interacting with atomic hydrogen, we found trains of UHCP's with width of each HCP down to  $\tau_p = 650 \text{ as}$  and intensity up to  $I_{HCP} = 4.2 \times 10^{12} \text{ W/cm}^2$ . Depending on the length of the driving field, we found UHCP trains from the few-cycle regime up to 30 cycles long. Moreover, the gas target dependence was studied within the single-active electron approximation for argon, yielding similar results as for hydrogen.

Future work will focus on studies necessary for the experimental realization of the protocol such as the characterization of the UHCP pulse, for example, by the FROG CRAB technique (frequency resolved optical gating for complete reconstruction of attosecond burst) [19], and methods for controlling intensities and phases of the components of the driving field present in the output.

## ACKNOWLEDGMENTS

This work was supported by the Austrian FWF under Grant No. SFB-016. Valuable discussions with A. Baltuška, M. Lezius, and V. Yakovlev are gratefully acknowledged.

- [1] M. Hentschel, R. Kienberger, Ch. Spielmann, G. A. Reider, N. Milosevic, T. Brabec, P. Corkum, U. Heinzmann, and M. Drescher, *Nature* (London) **414**, 509 (2001).
- [2] R. Kienberger, E. Goulielmakis, M. Uiberacker, A. Baltuska, V. Yakovlev, F. Bammer, A. Scrinzi, Th. Westerwalbesloh, U. Kleinberg, U. Heinzmann, M. Drescher, and F. Krausz, *Nature* (London) **427**, 817 (2004).
- [3] P. M. Paul, E. S. Toma, P. Breger, G. Mullot, F. Augé, Ph. Balcou, H. G. Muller, and P. Agostini, *Science* **292**, 1689 (2001).
- [4] D. G. Arbó, C. O. Reinhold, J. Burgdörfer, A. K. Pattanayak, C. L. Stokely, W. Zhao, J. C. Lancaster, and F. B. Dunning, *Phys. Rev. A* **67**, 063401 (2003).
- [5] C. Wesdorp, F. Robicheaux, and L. D. Noordam, *Phys. Rev. Lett.* **87**, 083001 (2001).
- [6] J. Ahn, D. N. Hutchinson, C. Rangan, and P. H. Bucksbaum, *Phys. Rev. Lett.* **86**, 1179 (2001).
- [7] S. Yoshida, C. O. Reinhold, E. Persson, J. Burgdörfer, and F. B. Dunning, *J. Phys. B* **38**, S209 (2005).
- [8] S. Yoshida, C. O. Reinhold, P. Kristöfel, and J. Burgdörfer, *Phys. Rev. A* **62**, 023408 (2000).
- [9] E. Persson, S. Yoshida, X. M. Tong, C. O. Reinhold, and J. Burgdörfer, *Phys. Rev. A* **68**, 063406 (2003).
- [10] J. Burgdörfer, *Nucl. Instrum. Methods Phys. Res. B* **42**, 500 (1989); M. Melles, C. O. Reinhold, and J. Burgdörfer, *ibid.* **79**, 109 (1993); C. O. Reinhold, J. Burgdörfer, M. T. Frey, and F. B. Dunning, *Phys. Rev. Lett.* **79**, 5226 (1997).
- [11] R. R. Jones, D. You, and P. H. Bucksbaum, *Phys. Rev. Lett.* **70**, 1236 (1993).
- [12] E. Persson, S. Puschkinski, X.-M. Tong, and J. Burgdörfer, in *Ultrafast Optics IV*, edited by F. Krausz *et al.*, Springer Series in Optical Sciences Vol. 95 (Springer, New York, 2004), pp. 253.
- [13] N. H. Shon, A. Suda, and K. Midorikawa, *Phys. Rev. A* **62**, 023801 (2000).
- [14] T. Brabec and F. Krausz, *Phys. Rev. Lett.* **78**, 3282 (1997); M. Geissler, G. Tempea, A. Scrinzi, M. Schnürer, F. Krausz, and T. Brabec, *ibid.* **83**, 2930 (1999).
- [15] T. Brabec and F. Krausz, *Rev. Mod. Phys.* **72**, 545 (2000).
- [16] X.-M. Tong and S.-I. Shu, *Chem. Phys.* **217**, 119 (1997).
- [17] W. Zhao, J. C. Lancaster, F. B. Dunning, C. O. Reinhold, and J. Burgdörfer, *J. Phys. B* **38**, S191 (2005).
- [18] H. G. Muller and F. C. Kooiman, *Phys. Rev. Lett.* **81**, 1207 (1998).
- [19] P. Johnsson, R. Lopez-Martens, S. Kazamias, J. Mauritsson, C. Valentin, T. Remetter, K. Varju, M. B. Gaarde, Y. Mairesse, H. Wabnitz, P. Salieres, P. Balcou, K. J. Schafer, and A. L'Huillier, *Phys. Rev. Lett.* **95**, 013001 (2005).